**Proceedings of ASME Turbo Expo 2011**
**GT2011**
**June 6-10, 2011, Vancouver, British Columbia, Canada**

# GT2011-45999

# EXPERIMENTAL INVESTIGATION OF TURBOCHARGER ROTOR BEARING SYSTEM

**Ankur Ashtekar**
Purdue University
West Lafayette, IN, USA

**Farshid Sadeghi**
Purdue University
West Lafayette, IN, USA

**Garry Powers**
Caterpillar Inc
Lafayette, IN, USA

**Kevin Mantel**
Caterpillar Inc
Lafayette, IN, USA

**Robert Griffith**
Caterpillar Inc
Peoria, IL, USA

## ABSTRACT

The objectives of this investigation were to design and construct a high speed turbocharger test rig to measure dynamics response of angular contact ball bearing rotor system, and to evaluate the performance of angular contact ball bearings as a replacement to conventional journal bearings in turbocharger systems. A test rig was designed and developed to operate at speeds up to 70,000 rpm. The rotating components (i.e. turbine wheels) of the turbocharger test rig were made to be dynamically similar to an actual turbocharger. Proximity sensors were used to record the turbine wheel displacements while accelerometers were used to monitor the rotor vibrations. A radio telemetry based wireless temperature sensor was designed and installed on the bearing cage. The in-situ temperature sensor monitored and recorded the bearing condition in real time. The rotor dynamic results obtained from the turbocharger test rig were used to corroborate with an analytical model developed simulate the turbocharger rotor system. The turbocharger test rig was then used to examine the dynamic response of the turbocharger. The rotor displacements and bearing temperatures were recorded and analyzed to study the effects of bearing preloading and rotor imbalance on the turbocharger ball bearing rotor system.

## INTRODUCTION

Turbochargers have commonly been equipped with journal bearings to support the turbines and rotor assembly. However, recently hybrid ceramic ball bearings have become popular as a replacement for journal bearings in turbochargers. Wang [1], in his review of ceramic bearing technology, points out that the hybrid ceramic bearing can provide better acceleration response, lower torque requirement, lower vibrations and lower temperature rise than journal bearings. Hybrid ceramic ball bearings contain steel inner and outer races, ceramic balls and usually a machined cage. Ceramic balls, as compared to their steel counter parts, are lighter, smoother, stiffer, harder, corrosion resistant, and electrically resistant. These fundamental characteristics allow for a wide range of performance enhancements in bearing rotor system. Ceramic balls are particularly well suited for use in harsh, high temperatures and/or corrosive environment. Therefore, hybrid ceramic bearings are ideal for turbocharger applications. Tanimoto et al. [2] have employed hybrid ceramic bearings in small, automotive turbochargers. However, challenges still remain for high speed, high output turbochargers which demand large bore bearings operating at speeds as high as 70,000 rpm. As the bearing size increases, the dynamics of the bearing rotor system becomes critical for comprehensive design and satisfactory operation of the turbocharger.

A number of investigators have attempted to experimentally analyze the dynamics of bearing rotor system. Adiletta et al. [3] and Dietl et al. [4] built experimental setups to gain knowledge of dynamics of bearing rotor systems operating at moderately low speeds (<10,000 rpm). However, turbocharger bearing rotor analysis presents unique challenges as the rotor can operate at speeds as high as 70,000 rpm. Most of the commonly used electric motors or IC engine based drive systems are limited to speeds below 20,000 rpm. Therefore, traditionally, the turbocharger test setups are designed and constructed around an engine test cell where the rotor is driven by hot exhaust gases from the engine. However, engine tests restrict sensor access to the rotor and the bearings, making it difficult to monitor the actual dynamics of bearing rotor system. Holt et al. [5] used a compressed air set up to eliminate the hot exhaust gas supply lines and the cooling water circuit in order to provide a better access to the bearing rotor system. However, access to the rotor is still limited by the compressor and turbine shrouds necessary for aerodynamic action of the turbine and compressor blades.

In this investigation a turbocharger test rig (TTR) was designed and developed to evaluate bearing and rotor system at various speeds. The rotor displacements, vibrations, speed were recorded and analyzed to obtain knowledge of the turbocharger bearing rotor dynamics. A model has also been developed to represent the turbocharger test rig bearing rotor system. The model combines a discrete element bearing model and a component mode synthesis rotor model to simulate the dynamics of the bearing rotor system. The results obtained from the model were corroborated with the experimental results.

## EXPERIMENTAL INVESTIGATION

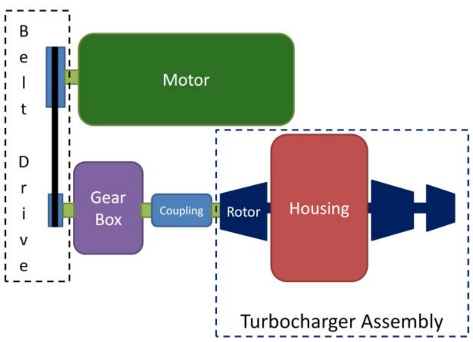


**(a)**

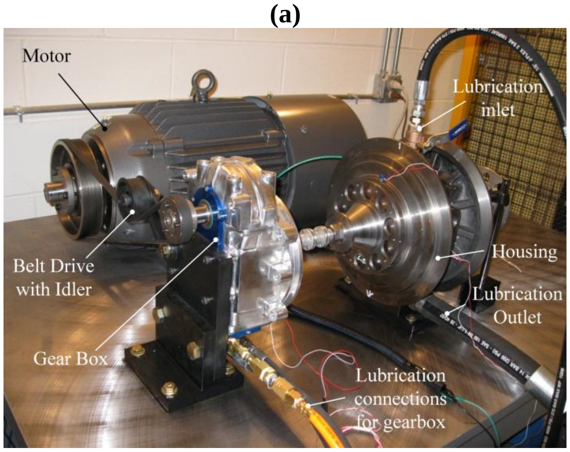


**(b)**

**Figure 1: Turbocharger Test Rig**

A 5000 rpm, 20 HP vector drive electric motor coupled to a belt pulley system and a gear box is used to drive the turbo charger test rig up to 70,000 rpm. The belt-pulley drive is used to increases the motor speed by 3.5 times. The output pulley drives a gearbox, which further increases the speed by another 4.21 times. The gearbox and the turbocharger assembly are coupled through a high speed flexible disc coupler. The assembly is aligned using a laser assisted system. The test rig along with its lubrication system is operated inside a reinforced room and monitored from a remote station through a set of wireless routers and cameras. In the following sections various attributes of the test rig are discussed.

**Turbocharger Assembly:** Figure 1 provides details of the bearing rotor assembly. The turbocharger rotor is supported by two back-to-back angular contact ball bearings. The two bearings used in the rig have a single one piece outer race which is supported inside the bearing housing by a pressurized squeeze film damper. An anti-rotation pin restricts the motion of the outer race about and along the axis of shaft rotation (i.e. X-axis). Two feed through holes in the outer race are used to supply oil to the bearing.

**Rotor Design:** The turbocharger has turbines which are used to rotate the rotor and drive the centrifugal compressors which supply pressurized air to the combustion chamber. This operation is entirely dependent on aerodynamic action of the blades on the turbine and the compressors. However, in this study, turbine and compressors were replaced with equivalent wheels which do not have blades and therefore do not generate any aerodynamic forces. This significantly reduces the complexity associated with the air circulation and discharge to operate the turbocharger test rig. A 20HP electric motor was used to drive the bearing rotor system at full speed under desired test conditions. The wheels were designed to have the same mass, CG location, and moment of inertia as the original rotor assembly. Table 1 contains a comparison between the rotors used in actual turbocharger and the wheels used in this investigation. Please note that the values have been non-dimensionalized with respect to the turbocharger rotor values.

**Table 1: Turbocharger (TC) rotor and equivalent wheel comparison**

| | Turbine | | LP Compressor | | HP Compressor | |
|---|---|---|---|---|---|---|
| | TC | Wheel | TC | Wheel | TC | Wheel |
| Mass | 1 | 0.9956 | 1 | 1.0033 | 1 | 0.9969 |
| CG | 1 | 0.9981 | 1 | 0.9976 | 1 | 0.9971 |
| Mass Moment of Inertia | 1 | 0.9997 | 1 | 1.0005 | 1 | 1.0012 |

Also, to verify that the equivalent wheels and the actual turbocharger rotor have similar modal response, experimental modal analysis was performed on the actual turbines and the equivalent wheels using the Multiple Input Multiple Output approach. The comparison of natural frequencies is shown in Table 2. Please note that the values have been non-dimensionalized with respect to the turbocharger rotor values.

Figure 3 depicts the placement of the proximity sensors around the rotor to measure circumferential displacements.

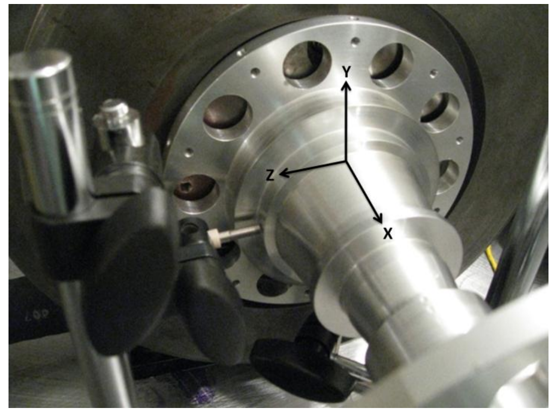


**(a)**

**(b)**

**Figure 3: Proximity sensors in Y axis and Z axis**

**Table 2: Modal response of turbocharger**

| | Mode 1(Hz) | Mode 2(Hz) | Mode 3(Hz) | Mode 4(Hz) | Mode 5(Hz) |
|---|---|---|---|---|---|
| Turbocharger Assembly | 1 | 1 | 1 | 1 | 1 |
| Equivalent Assembly | 0.9710 | 0.9344 | 0.9127 | 0.9862 | 0.9863 |

**Rotor and Component Balance:** The equivalent rotor assembly was dynamically balanced to ISO G2.5 standard. Each rotor part was independently balanced before assembly and later the complete rotor assembly was also balanced to the same specifications. Nevertheless, the rotor was designed to allow for adding external weights around the periphery to create controlled imbalance. Each plane has 12 equally spaced threaded holes, as shown in Figure 2, which can be plugged to add small amounts of controlled imbalance to the rotor and observe its effect on the rotor and bearing dynamics.

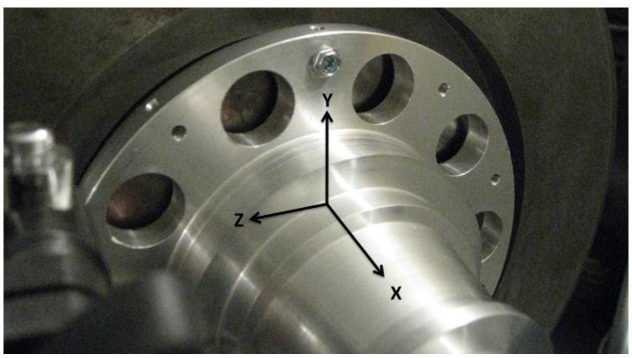


**Figure 2: Introduction of Imbalance to the Rotor**

**Lubrication System:** A recirculating lubrication system was used to supply pressurized oil (50 psi) to the turbocharger test rig. The lubricating oil is pumped through a heat exchanger to maintain the desired lubricant temperature before it is supplied to the turbocharger bearings, squeeze film damper and the gear box. The cooled oil is then filtered to remove contaminants particles of 10 µm and larger. Approximately 1 gallon per minute of oil is supplied to the turbocharger bearing housing where it forms a pressurized squeezed film damper to support the bearing outer race inside the housing. Feed through holes on the bearing outer race directs part of this oil to the bearings. The lubricating oil is then drained back to the sump. The gear box used in the TTR requires oil mist lubrication and therefore the oil is mixed with air and supplied to the gearbox at 20 psi. The oil mist exhaust from the gear box is passed through an oil trap to separate oil from air. The separated oil is then drained back to the sump.

**Displacement Proximity Sensors:** Rotor displacements were measured using non-contact inductive proximity sensors. Four sensors were used to measure the circumferential (YZ) and out of plane (XY and XZ) displacements of the rotors.

**Temperatue Sensors:** A radio telemetry based temperature sensor was developed to measure the temperature inside the bearing during operation. Traditional thermocouples only provide temperature of the bearing housing and are not an accurate measurement of the temperature inside the bearing. Also the housing has large heat capacity which acts as heat sink. Therefore small temperature variations are not detected by thermocouple mounted on the housing.

The telemeter has two components: an active transceiver and a passive sensor. The passive sensor is an inductor-capacitor resonator. The capacitor is temperature-sensitive and is bonded to the cage with an electrically-insulating, but thermally-conductive epoxy. The inductor is a circular wire loop that is electrically connected in parallel to the capacitor, forming a resonator. As the temperature of the capacitor changes, its capacitance will also change, thereby shifting the natural frequency of the resonator. This passive sensor is then magnetically coupled through the inductor with the transceiver.

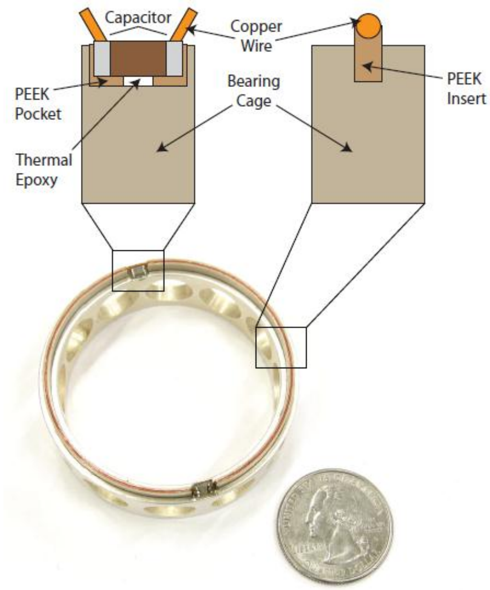


**Figure 4: Image of Modified Bearing Cage with Cutaway Diagram. The Quarter is shown for Scale.**

The passive sensor was fabricated on a polyetheretherketone (PEEK) ring that was pressed into a modified bearing cage. A cavity for the sensing capacitor was milled into the material extending into the cage and a shallow hole drilled through and filled with conductive epoxy. The sensing capacitor was then bonded into the cavity. A channel was cut onto the top surface of the PEEK ring and a wire was pressed into it. Both ends of the wire were soldered directly to the sensing capacitor, creating the resonator.

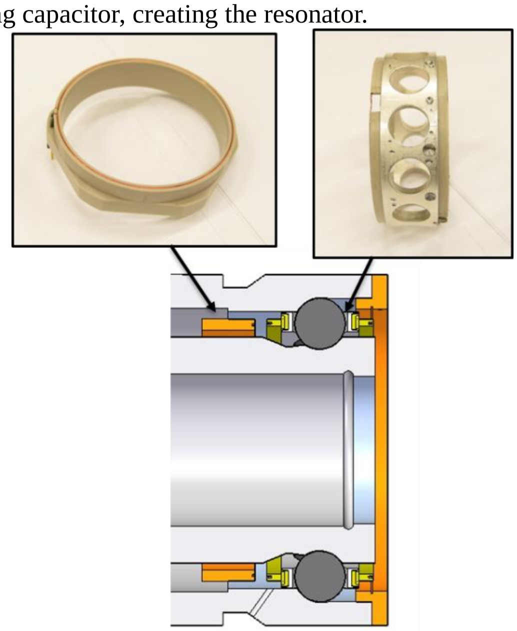

**Figure 5: Sensor Package**

A photograph of the completed sensor as well as a cross-sectional diagram is provided in Figure 4.

The transceiver was also fabricated out of a PEEK ring with a channel milled out for the inductor wire, much like the passive sensor. A 1 meter coaxial cable was soldered to the ends of the inductor so as to allow an interface to the telemeter from outside of the bearing housing. This ring was then mounted on the inside of the bearing with the inductor placed 3mm away from the inductor on the cage sensor. Figure 5 shows the finished components of the telemeter and how they fit inside of the housing. The coaxial cable is not shown in this case. Sensor calibration procedure and relevant data has been published elsewhere [6].

National Instruments data acquisition hardware and custom LabVIEW software program were used to collect and analyze the displacement data.

Similar to Adiletta et al. [3, 7], results from the experimental TTR investigation were corroborated with the displacements predicted by the analytical investigation. Once good correlation was obtained between the results, the effects of bearing preloading and rotor imbalance on turbocharger bearing were examined.

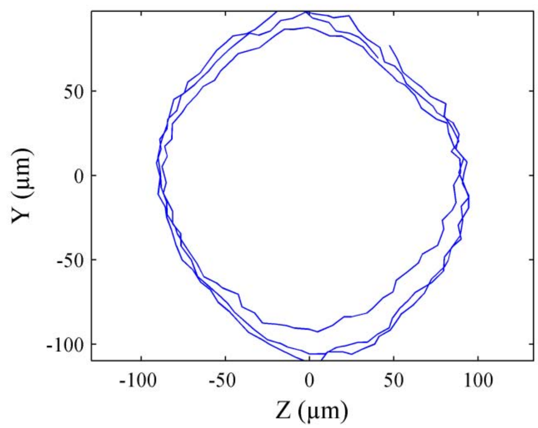


(a) Turbocharger Test Rig

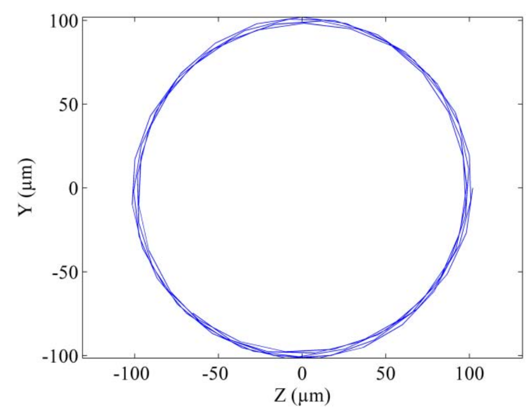


(b) Analytical model

**Figure 6: LP Displacement (µm) at 1000 rpm**

## RESULTS AND DISCUSSION

**Experimental and Analytical Results Corroboration:** Rotor displacements predicted by the Dynamic Bearing Rotor Model were corroborated with the results obtained from the Turbocharger Test Rig. The rotor and support bearing specifications used in the DBRM and TTR are given in Table 1 and Table 3 respectively.

**Table 3: Bearing Specifications**

| | |
|---|---|
| **Bearing Type** | Ceramic Hybrid Angular Contact |
| **Bore & O.D.(mm)** | 28 & 60 |
| **No. of Balls** | 12 |
| **Race Material** | M-50 NiL |
| **Ball Material** | $Si_3N_4$ |
| **Cage material** | Aluminum |
| **Contact angle** | 25 |

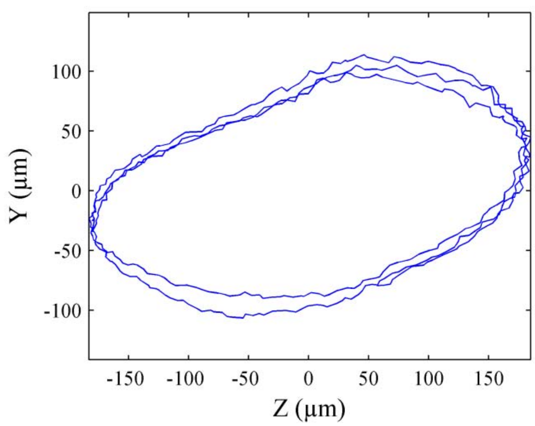


(a) Turbocharger Test Rig

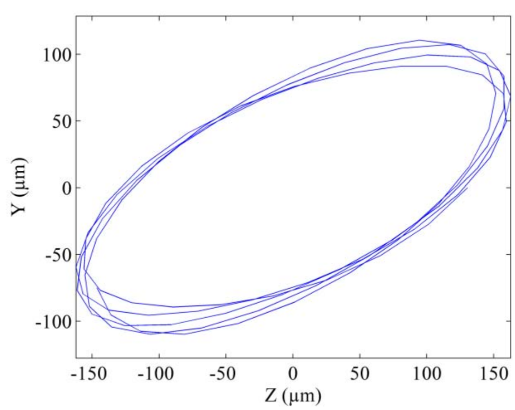


(b) Analytical model

**Figure7: LP displacement (μm) at 5000 rpm**

As shown in Figure 1, low pressure (LP) compressor wheel is farthest from the bearing. Because of its large overhang it undergoes maximum displacements during operation. Therefore, displacement of the LP wheel was measured to obtain critical knowledge of the rotor system. The experimental displacement results were then corroborated with the analytical results. The dynamic simulation begins with rotor at rest and exponentially increasing the rotor speed such that after a period of five milliseconds the rotor achieves the desired steady-state rotational speed.

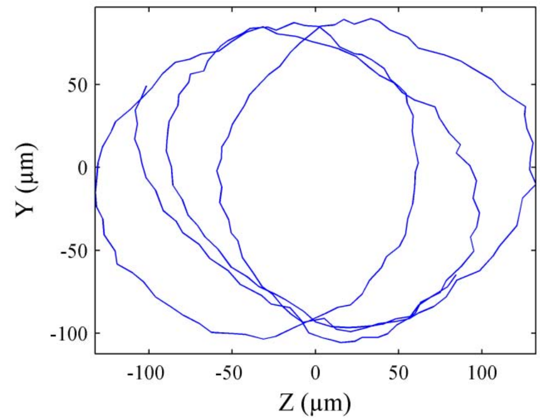


(a) Turbocharger Test Rig

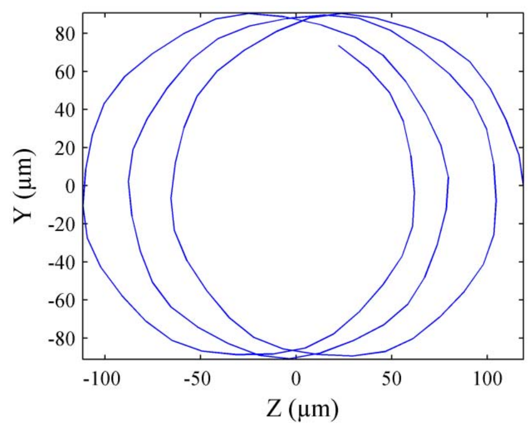


(b) Analytical model

**Figure 8: LP displacement (μm) at 10000 rpm**

The orbital displacement of the LP wheel was obtained from the model and compared with the measured results obtained from the TTR operating at various speeds. Figure 6 through Figure 9 illustrate the results of this comparative investigation. Figure 6 depicts the result for the slow speed case of 1000 rpm. In this case, the LP wheel displacement is of circular shape and it is predominantly caused by the bearing and rotor run-outs. No significant effects of rotor flexibility are observed (Figure 6a). Figure 7 illustrates the results for the 5000 rpm case. At this higher speed condition, the LP wheel motion becomes elliptical as in contrast to the lower speed case of Figure 6, where the motion was primarily circular. This elliptical shape is principally due to the flexibility of the rotor system. As the speed increases further, the rotor modes significantly affect the LP wheel displacement motion.

Figure 8 depicts the results for the 10,000rpm case. Rotor is observed to sweep horizontally. The LP wheel displacement is a combination of rotor sweep and circular rotor run-out motion.

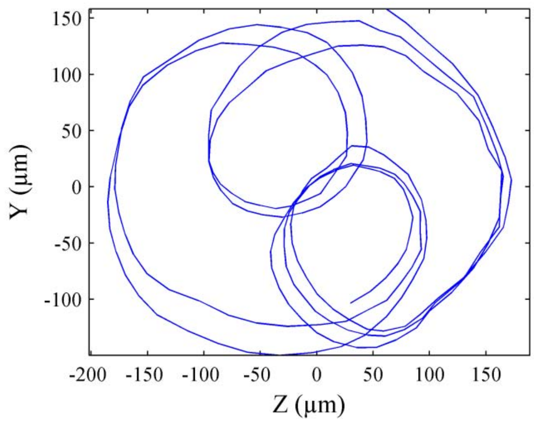

(a) Turbocharger Test Rig

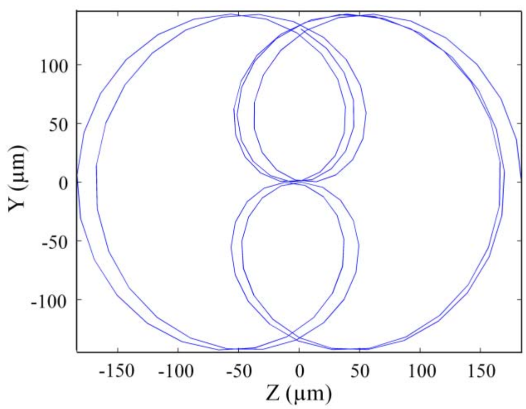

(b) Analytical model

**Figure 9: LP displacement (µm) at 20000 rpm**

In Figure 9, at 20000 rpm the rotor motion is vertical. High frequency vertical motion coupled with run-out motion results in looping motion of the LP wheel. As the rotor speed increases, different mode shapes start dominating and affect the LP compressor wheel vibration. This results in a specific shape of the orbital path. It can be seen that the analytical results and experimental results match to corroborate the results of this investigation.

**Imbalance:** In high speed applications, imbalance causes significant vibration and centrifugal forces on various components of the bearing. Even minor imbalance severely affects the rotor dynamics. Figure 10 and Figure 11 show a comparison of LP compressor wheel orbital paths for balanced and imbalanced cases of the TTR. The operating conditions for each case are as shown in the Table 5.

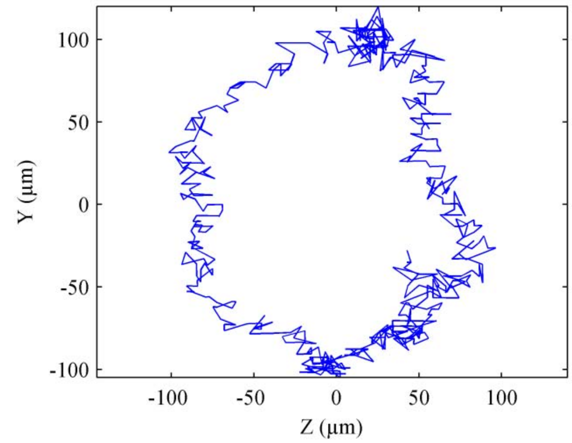

(a) Balanced

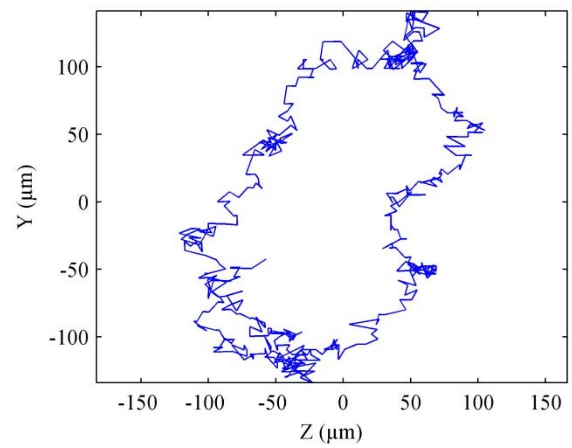

(b) Imbalanced

**Figure 10: Rotor displacement at 1350 rpm with 20gm-mm imbalance**

Figure 10 depicts the case when the rotor is operating at 1350 rpm. Please note, the high frequency noise seen in this figure originated from the gearbox. The problem was later resolved and thus noise is not present in figure 6-9. Nevertheless, it can be noted that the magnitude of LP wheel radial displacement increased from 110 µm to 140 µm when imbalance is introduced.

**Table 5: Bearing operating conditions**

| | |
|---|---|
| **Imbalance (gm-mm)** | 20 |
| **Imbalance location** | LP Compressor Wheel |

Figure 11 depicts the case at 2700 rpm, in this case the LP wheel radial displacement increased from 100 µm to 300 µm for the same amount of imbalance. In both the cases, LP wheel displacement shape also changed significantly. The results demonstrate that the vibrating modes and its amplitudes are considerably different for the imbalanced rotor. This is because the imbalance acts as a periodic external force and excites different modes of the rotor system. These changes in rotor behavior are transmitted to all the bearing components. These effects are severe in bearings operating at high speeds and have significant effect on bearing life.

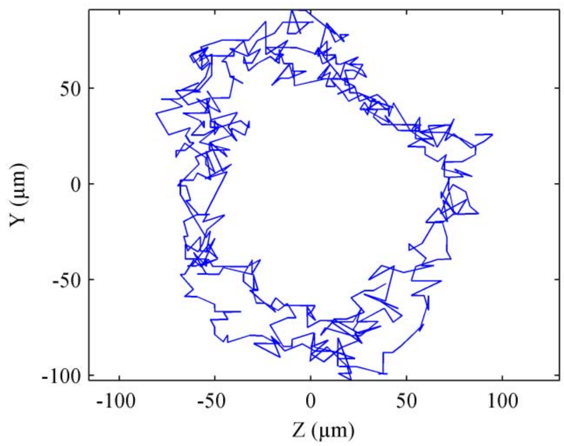

(a) Balanced

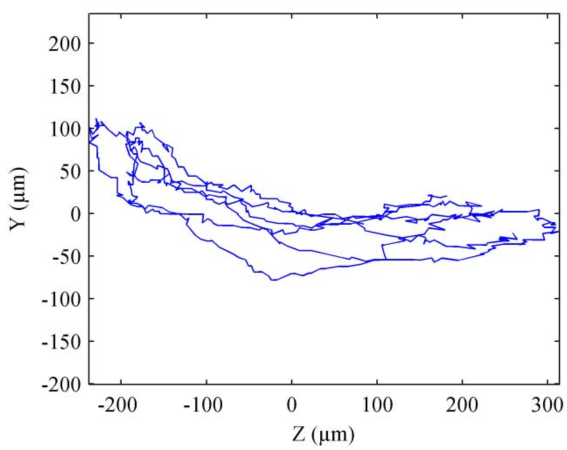

(b) Imbalanced

**Figure11: Rotor displacement at 2700 rpm with 20gm-mm imbalance**

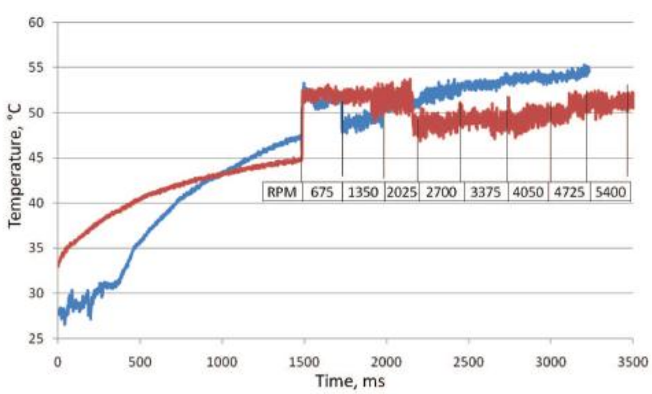


**Figure 12: Bearing Temperature for Balanced (red) and Imbalanced (blue) rotor**

In Figure 12, a plot of temperature data at various speeds for a balanced and an imbalanced rotor is compared. The operating temperature of the bearing for an imbalanced rotor is consistently higher than the temperature observed for a balanced rotor. This is expected as the imbalanced rotor has a much more aggressive motion than a balanced rotor. The motion is transmitted to the bearing and results in excessive sliding or rubbing of the balls, leading to excessive friction losses. In the case of 4750 RPM, a 5±C increase in operating temperature was observed compared to a balanced rotor case.

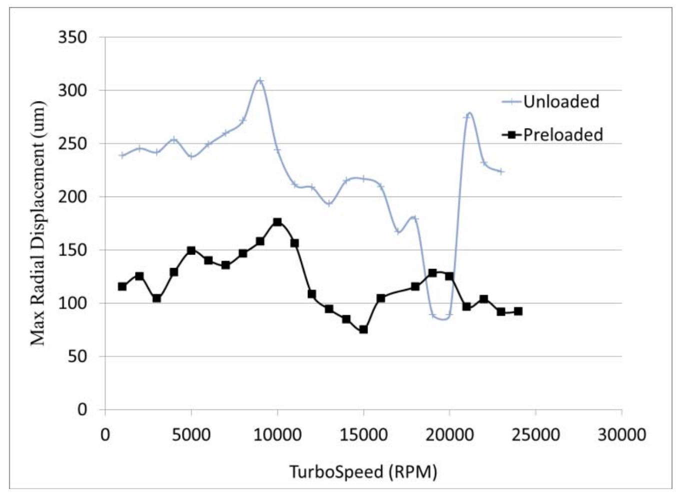


**Figure:13 Radial Displacement of LP Wheel for Unloaded and Preloaded Bearing**

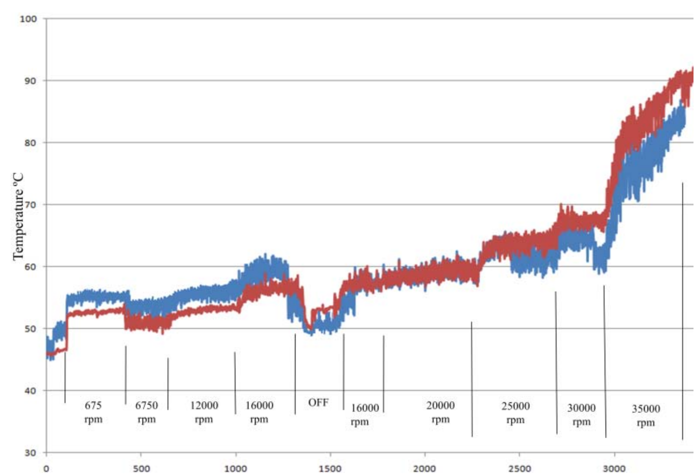


**Figure 14: Bearing Temperature for Unloaded (red) and Preloaded (blue) bearing**

**Preloading:** Figure 13 shows the effect of bearing preloading on bearing-rotor dynamics. The TTR was operated for two cases, one with bearing preloaded to maximum value and one without any preloading. Maximum radial displacement of LP wheel was measured with proximity sensors and plotted against speed. Larger is the displacement, higher is the instability. It can be noted that the radial displacements for unloaded case are considerably higher than the displacements measured for the preloaded case. Figure 14 shows the temperature inside the bearing for similar cases. At high speeds the temperatures are higher for unloaded case. However, at low speeds the preloaded bearing operates at higher temperature. This is primarily due to the high contact pressures between ball and race due to preloading. As the speed increases, centrifugal force relives some of the contact pressure in preloaded bearing. However, in unloaded bearing, the centrifugal load completely unseats the ball from inner race and results in sliding and slipping between ball and inner race. Thus the temperature for unloaded bearing increases at higher speeds. Nevertheless, the bearing under consideration was found to have insufficient preloading mechanism and thus at high speeds, both the bearings loose considerable traction with the inner race. This results in sliding and slipping in both the cases and the temperature of the bearing shows a sharp rise at high speeds above 30,000 rpm.

## CONCLUSIONS

Investigation into replacing journal bearings of a high speed turbocharger with hybrid ceramic ball bearings requires experimental test setup as well as a detailed analytical model of bearing rotor dynamics. In this investigation a high speed turbo charger test rig was designed and developed. The turbocharger rotors were replaced with equivalent wheels developed to eliminate aerodynamic forces of turbocharger rotor. This considerably reduced the power required to drive the test rig at high speeds. A telemetry based temperature sensor was developed to measure the temperature inside the bearing during operations. The test rig was also equipped with proximity sensors to measure motion of LP wheel at various speeds. The analytical results and experimental results were corroborated for a range of operating speeds. The test rig was also used to investigate the vibration and motion of LP wheel when imbalance was introduced in the system. Also study was performed to determine the effect of bearing preload on turbocharger bearing – rotor performance. However, the bearing under investigation showed considerable instability even at low speeds due to improper preloading, restricting the acceptable operating speeds to lower speeds. Effect of aerodynamic loading and temperature gradients on preloading (and rotor dynamics) would be interesting and thus the rig will be upgraded in the future to include these effects. Nevertheless, the results from the current setup indicate that correct bearing preload, based on rotor-bearing dynamics and bearing temperature, is important for turbocharger applications to operate optimally at wide range of speeds.

## ACKNOWLEDGMENTS

The authors would like to express their deepest appreciation to Caterpillar Inc. for their support of this project.

## REFERENCES

[1] Wang L., Snidle R., and Gu L., 2000, "Rolling contact silicon nitride bearing technology: a review of recent research," Wear, **246**(1-2), pp. 159-173.

[2] Tanimoto K., Kajihara K., and Yanai K., 2000, "Hybrid ceramic ball bearings for turbochargers," SAE Paper 2000-01-1339, pp. 1-14.

[3] Adiletta G., Guido A., and Rossi C., 1997, "Nonlinear dynamics of a rigid unbalanced rotor in journal bearings. Part II: Experimental analysis," Nonlinear Dynamics, **14**(2), pp. 157-189.

[4] Dietl P., Wensing J., and Nijen G. C., 2000, "Rolling bearing damping for dynamic analysis of multi-body systems—experimental and theoretical results," Proc. I. Mech. E., Part K: J. Multi-body Dynamics, **214**(1), pp. 33-43.

[5] Holt C., San Andres L., Sahay S., Tang P., La Rue G., and Gjika K., 2005, "Test Response and Nonlinear Analysis of a Turbocharger Supported on Floating Ring Bearings," ASME J. Vibr. Acoust., **127**(2), pp. 107-115.

[6] Ashtekar, A, and A Kovacs., Sadeghi, F.; Peroulis, D., 2010 “Bearing cage telemeter for the detection of shaft imbalance in rotating systems.” IEEE Radio and Wireless Symposium, pp. 5-8.

[7] Adiletta G., Guido A., and Rossi C., 1997, "Nonlinear dynamics of a rigid unbalanced rotor in journal bearings. Part I: Theoretical analysis," Nonlinear Dynamics, **2**, pp. 57-87.